Elektrotechnik und Informationstechnik 119(4), 114-119 (2002)

Performance Analysis of a Space-Based Multiple-Telescope Nulling Interferometer for DARWIN

Oswald Wallner IEEE*, Klaus Kudielka IEEE†

Abstract

The European Space Agency's infrared space interferometer DARWIN is dedicated to the investigation of Earth-like extrasolar planets orbiting bright stars. A multi-aperture interferometer fed by free-flying telescopes allows spectroscopic analysis of the weak planet signal which could give hints on the possibility of the existence of Earth-like life. However, for a Sun/Earth-like constellation at an interstellar distance of some 50 light years, a star light suppression of about $60dB$ is required to make the weak planet signal visible.

In this paper we investigate the nulling capability of a space-based Robin Laurance interferometer in the case of stochastic disturbances of the array geometry and of stochastic alignment errors of the optical components, which both will be actively controlled. Mismatch of amplitude transmission, optical path length, and polarization transmission among the interferometer arms is taken into account.

We numerically analyze Sun/Earth-like constellations in the wavelength range of 6 to 18 microns and calculate the expected value of the star light rejection ratio for the Robin Laurance geometry. It is shown that maximum standard deviations of only $\sigma_p = 2nm$ and $\sigma_A = 5 \cdot 10^{-4}$ for the differences in optical path length and amplitude transmission can be allowed to obtain a rejection ratio of $R = 60dB$. These and other exemplary numerical results confirm the extreme requirements for interferometer uniformity and give a quantitative insight into the dependence of the attainable rejection ratio on individual and/or combined interferometer imperfections.

*Dipl.-Ing. Oswald Wallner, Institut für Nachrichtentechnik und Hochfrequenztechnik, Technische Universität Wien, Gusshausstrasse 25/389, A-1040 Wien, E-mail: oswald.wallner@ieee.org

†Dr. Klaus Kudielka, Contraves Space AG, Schaffhauserstrasse 580, CH-8052 Zürich, E-mail: klaus.kudielka@ieee.org

1 Introduction

The objective of the European Space Agency's infrared space interferometry mission called DARWIN is to detect and analyze Earth-like extrasolar planets [1]. The prospect is to detect absorption lines of potential life indicators, like H_2O, O_3, or CO_2, by spectroscopic analysis of the radiation received from the planet in the infrared wavelength regime of 6 to 18 microns. The investigations, to be performed by an instrument positioned in an orbit at the second Lagrangian point, are eyed on Sun/Earth-like constellations at interstellar distances of some 50 light years.

The instrumental problems to be solved stem from the close neighborhood of the star and the planet and from the high contrast between the two radiation sources. A nulling interferometer as suggested for DARWIN, in principle provides both a high angular resolution to separate the planet from the star and a strong rejection of the star light. However, the large wavelength range of operation and the extreme requirements on interferometer uniformity are highly challenging demands on the interferometric instrument.

In this paper we investigate the nulling capability of a space-based Robin Laurance interferometer in the case of stochastic disturbances of the array geometry and of stochastic alignment errors of the optical components. We establish a system model describing the parameters influencing the rejection performance and analyze the suppression of the star light in the case of individual and/or combined stochastic interferometer imperfections.

2 The Robin Laurance nulling interferometer

In a nulling interferometer the light arriving from slightly different directions experiences significantly different transmissions, when propagating through an interferometer as shown in Fig. 1 [2]. In the simplest arrangement, the sum of star and planet waves incident in the observation plane is received by two identical telescopes. One of the resulting signals is then changed in phase, and finally both signals are superimposed to obtain interference. Destructive interference for the star signal is obtained for a relative phase shift of half a wavelength between the two interferometer

arms. In case of adjustment of the telescope positions, i.e. for a spacing of $\lambda_0/(2\Theta)$, the planet signal experiences constructive interference. As the input signals are not monochromatic, the required phase relation to null the on-axis star has to be realized by an achromatic phase shifter, i.e. independent of the input signal wavelength λ. The optimum condition for the telescope spacing obviously can be only fulfilled for a single wavelength, the design wavelength λ_0, which should be chosen as the smallest wavelength of the interval considered.

In practice, the interferometer will consist of an array of more than two telescopes, where the number and the geometry depend on the required rejection ratio and on the star/planet constellation. Several geometries have been analyzed in the past [3, 4]. Presently, the hexagonal Robin Laurance configuration seems to be the most suitable one [5]. An artist's conception is shown in Fig. 2 [6]. The Robin Laurance configuration consists of six equal, free flying telescopes arranged in a hexagonal geometry, one in-plane hub satellite comprising the beam combiner, and possibly one out-of-plane master satellite. The advantage of this concept compared to the previous ones is that it allows internal switching of the interferometer's spatial transmission maps, which is required for distinguishing between exozodiacal dust clouds and planetary signals. Only four telescopes are operated at a time to form a nulling interferometer. Figure 3 shows the geometries and the source plane transmission maps of the three resulting arrangements.

In our investigations we arbitrarily define the planet's Cartesian coordinates as $(x_p, y_p) = (1AU, 0)$, where AU denotes an astronomical unit (the mean distance between Sun and Earth), and exemplarily analyze the interferometer as shown in the center column of Fig. 3. In order not to attenuate the already weak planet signal, the planet position should coincide with an interference maximum of the transmission map. This is attained if the diameter d of the hexagon fulfills the condition $d = 2\lambda_0 L/x_p = 40m$, where $\lambda_0 = 6\mu m$ is the smallest wavelength of interest and $L = 50LY$ is the distance between telescope array and star (LY denotes light year).

3 Performance analysis model

In the following we investigate the impact of imperfections on the rejection performance of a single-mode, multi-telescope nulling interferometer with a co-axial beam combining scheme. The general structure of such an instrument is shown in Fig. 4. The incident radiation is coupled to the propagation medium (fiber or free-space optics) by means of the *receiving unit*, i.e. by a telescope. The sub-beams then are affected in phase by *achromatic phase shifters*, which establish the phase relation required for star light rejection, nominally independent of the wavelength. For deep nulling, uniformity in amplitude, optical path length, and state of polarization of the signals to be combined is absolutely necessary. To this end these properties of the sub-beams are adapted by *control units*, the control signals of which are derived from various sensor systems not shown here and from the overall output signal. In the *combining optics* the individual subbeams interfere, i.e. the output of the combining optics nominally carries only the planet signal. In the *processing unit* the actual science measurement is performed.

If all the system components work perfectly, nulling of the star light to the theoretical limit determined by the array geometry is possible. In a practical system, imperfections of the geometry and of optical components occur, leading to a reduced rejection capability. Individual errors concerning amplitude transmission, optical path length, and polarization transmission of all components or subsystems are added up to overall errors. This is allowed because the interferometer output consists only of a single spatial mode. Hence we do not analyze the influence of imperfections of individual optical components, but derive conditions the system has to fulfill as a whole.

The stellar and planetary sources are assumed to be flat, spatially incoherent Lambertian radiators located in the source plane (x_s, y_s), characterized by their spectral radiances $N_s(\lambda; x_s, y_s)$ and $N_p(\lambda; x_s, y_s)$, respectively, as given by Planck's law of radiation (the planet's albedo is assumed to be zero). Within the aperture plane (x_a, y_a), located at a distance of L from the source plane, the intensities due to the two sources approximately amount to $I_s = N_s A_s \triangle\lambda / L^2$ and $I_p = N_p A_p \triangle\lambda / L^2$,

respectively. The radiator's cross-sections in the source plane are denoted by A_s and A_p, and $\triangle\lambda$ is the optical bandwidth of the observer. The spectral radiances are assumed to be constant across the cross-section of each source and within the optical bandwidth.

The radiation incident upon the aperture plane is collected by several telescopes, influenced in amplitude, phase, and polarization, and finally superimposed co-axially to form a single output beam, which carries the optical power P_p due to the planet and P_s due to the star. As a result of the interferometer's high spatial selectivity and because of proper positioning of the telescopes and proper phasing of the sub-beams, the radiation due to the star experiences destructive interference while the radiation of the planet interferes constructively. The rejection ratio R is defined as the factor by which the star light is rejected when comparing the interferometer with a wide-field-of-view telescope, i.e.

$$\underbrace{\frac{P_p}{P_s}}_{>1} = R \cdot \underbrace{\frac{I_p}{I_s}}_{\ll 1} \quad . \tag{1}$$

For the design wavelength λ_0, where the planet signals experience perfect constructive interference, this definition is equal to the commonly used definition $R = P_c/P_d$, where P_c is the interferometer output power due to constructive interference of the star signals within both arms, and P_d is the output power due to destructive interference, i.e. if an achromatic phase shifter is present. For wavelengths other than λ_0 the planet signals do not experience perfect constructive interference. This additional degradation of the interferometer performance is also taken into account by the definition as given in (1).

For linearly polarized input radiation, the stochastic wave amplitude $\boldsymbol{A}$ of an N-arm single-mode interferometer of arbitrary geometry is given by the sum of the contributions $\boldsymbol{A}_n$ from the individual arms,

$$\boldsymbol{A}_n = \iint_{\mathbb{R}^2} M^*_{a,n}(x_a, y_a)\, \boldsymbol{E}_a(x_a, y_a)\, dx_a dy_a \quad , \tag{2}$$

where $\boldsymbol{E}_a$ is the stochastic optical input field, and $M_{a,n}$ is the complex, normalized eigenmode associated with arm n, both specified in the aperture plane. Since the interferometer output comprises a single spatial mode, any error in amplitude or phase transmission occurring within

arm n can be taken into account by $M_{a,n}$. Applying the Van Cittert-Zernike theorem [7], the average interferometer output power is given by

$$P = \langle |\boldsymbol{A}|^2 \rangle = \sum_{m=1}^{N} \sum_{n=1}^{N} \langle \boldsymbol{A}_m^* \boldsymbol{A}_n \rangle = \iint_{\mathbb{R}^2} \frac{N(\lambda; x_s, y_s)}{2} \triangle\lambda \cdot G(x_s, y_s)\, dx_s dy_s \quad , \tag{3}$$

with $G(x_s, y_s)$ denoting the interferometers receive characteristic backpropagated into the source plane. $G(x_s, y_s)$ is given as the squared modulus of the sum of all normalized eigenmodes, likewise backpropagated into (x_s, y_s). The factor 1/2 in Eq. 3 is due to the fact that only a single linear state of polarization is observed. Equation 3 shows that the average output power is the product of the radiance distribution of the source and the receive characteristic of the interferometer. Since the star is not infinitesimally small, the individual output wave contributions $\boldsymbol{A}_n$ are not perfectly correlated, i.e. $|\langle \boldsymbol{A}_m^* \boldsymbol{A}_n \rangle|^2 < \langle |\boldsymbol{A}_m|^2 \rangle \langle |\boldsymbol{A}_n|^2 \rangle$, and thus are not able to produce a perfect destructive interference. The star signal can be perfectly rejected only at a single point of $G(x_s, y_s)$.

The general case of unpolarized light can easily be modelled by a source emitting two orthogonal polarization modes $E_{s,x}$ and $E_{s,y}$, each being statistically independent of each other. The incident fields in the aperture plane are still statistically independent, i.e. $\langle \boldsymbol{E}_{a,x} \boldsymbol{E}_{a,y} \rangle = 0$. The derivation of the mean interferometer output power follows closely the method described before. However, since each state of polarization may be affected differently in each interferometer arm (taken into account by terms $M_{a,n,xx}$, $M_{a,n,yy}$) and even polarization crosstalk (characterized by $M_{a,n,xy}$,$M_{a,n,yx}$) may occur, the normalized mode field distribution, as introduced in Eq. 2, is a two-by-two matrix now. The average interferometer output power is given by Eq. 3, but now the receive characteristic is the sum of four different characteristics, $G = G_{xx} + G_{xy} + G_{yx} + G_{yy}$, each responsible for a certain combination of input and output state of polarization.

We thus may view Equation 3 as the general expression for the mean output power of a single-mode nulling interferometer. If we apply a paraxial approximation, and regard the planet as a point source and the star as a Lambertian radiator with constant spectral radiance $N_s(\lambda)$ within

its cross-section (a disk of radius a_s), the rejection ratio, defined in Eq. 1, becomes

$$R = \frac{G(x_p, y_p)}{\frac{1}{a_s^2\pi} \iint\limits_{x_s^2+y_s^2 \le a_s^2} G(x_s, y_s)\, dx_s dy_s} \quad . \tag{4}$$

In practice, some parameters characterizing the telescope array's receive characteristic $G(x_s, y_s)$ exhibit stochastic variations around their optimum values. This may be due to environmental influences or due to noise induced by active control loops which are needed to achieve the required parameter conformity. To assess their influence on the rejection capability, the pertinent parameters were modelled as Gaussian random variables and the average interferometer output power due to the star and the planet was calculated. For observation times much larger than the time constant associated with the stochastic variations, the rejection ratio, Eq. 4, may be estimated by a Monte Carlo analysis, i.e. by

$$R(\lambda) = \frac{\langle \boldsymbol{G}(\lambda; x_p, y_p) \rangle}{\frac{1}{a_s^2\pi} \iint\limits_{x_s^2+y_s^2 \le a_s^2} \langle \boldsymbol{G}(\lambda; x_s, y_s) \rangle\, dx_s dy_s} \approx \frac{\sum_i G_i(\lambda; x_p, y_p)}{\sum_i \frac{1}{a_s^2\pi} \iint\limits_{x_s^2+y_s^2 \le a_s^2} G_i(\lambda; x_s, y_s)\, dx_s dy_s} \quad , \tag{5}$$

where $G_i(\lambda; x_s, y_s)$ is the receive characteristic of interferometer realization i.

4 Statistical analysis

To numerically analyze the influence of various imperfections on the nulling capability of the interferometer we employ the general system model presented in Fig. 4. As already mentioned, we combine all errors in amplitude, phase, or polarization transmission of each interferometer arm. Each of these three errors is then actively compensated by an appropriate control unit – however, only up to a certain residual error.

Concerning the task of matching the states of polarization among the interferometer arms it is necessary to make some additional assumptions. It seems that an interferometer operating nominally in a single state of polarization is the most practicable one. In contrast to the general case where eight degrees of freedom per arm have to be actively controlled (especially if fibers are used as propagation medium), any error in polarization transmission is transformed into errors in

amplitude and phase. Consequently we model the polarization properties of the interferometer arms as follows: An input polarizer, characterized by its finite, deterministic extinction ratio and by a stochastic rotation around the optical axis, is mounted at the telescope. The path from the polarizer to the beam combiner is described by a deterministic birefringence, i.e. the optical path length difference between the desired and the undesired polarization axis. Any misalignment of the optics feeding the combiner is relatively uncritical and therefore neglected. At the interferometer output, a polarizer again filters the nominal state of polarization.

In the following we discuss the numerical results obtained for the Robin Laurance nulling interferometer (as shown in the center column of Fig. 3) with an array diameter of $40m$ and a telescope diameter of $1.5m$. The amplitude transmission factors of the individual arms are 1/6, 1/2 and 1/3. In two arms, a phase shift of half a wavelength is introduced. The distance between telescope array and star is 50 light years and the planet is positioned one astronomical unit from the star.

As the telescope array is optimized for the smallest wavelength of interest, i.e. $\lambda_0 = 6\mu m$, the interferometers receive characteristic is scaled by a factor of λ/λ_0 for other wavelengths. For wavelengths larger than the design wavelength, the receive characteristic is broadened, resulting in an increased rejection ratio – a perfectly aligned interferometer assumed. The reason is that although the radiation due to the planet does not interfere 100% constructively, the null at the star's center becomes broader which leads to a better rejection of the star light. For wavelengths smaller than the design wavelength, the receive characteristic is compressed, which results in both a decrease of the interferometer output power due to the planet and an increase of the interferometer output power due to the star. Hence, the rejection ratio decreases rapidly. With strong imperfections present, the rejection ratio also decreases with increasing wavelength.

We first analyzed the influence of single imperfections on the rejection performance and then calculate the combined effect of multiple imperfections. For the statistical analysis we modelled the error of each appropriate parameter as a zero-mean, Gaussian random variable. The standard deviation σ is assumed to be equal in each interferometer arm and the individual errors are statisti-

cally independent from each other. The following results are obtained by a Monte Carlo simulation using 1000 realizations $G_i(\lambda; x_s, y_s)$.

The extraordinary requirements on optical path length and amplitude transmission uniformity are shown in Fig. 5. Because for Sun/Earth-like constellations a rejection ratio of some $60dB$ is required [1], only standard deviations of about $\sigma_p = 2 \cdot 10^{-9}m$ for the optical path length error and $\sigma_A = 5 \cdot 10^{-4}$ for the field amplitude transmission error can be allowed. The wavelength characteristics, depicted in Fig. 6 and 7, show the expected behavior, namely an increase of R for very small errors and a decrease for large errors.

To analyze the influence of polarization mismatch, the influence of real polarizers and birefringence has been taken into account. Because the pertinent tolerances are very tight and thus proper rotation of each subtelescope has to be actively maintained, the angles α of the input polarizers are modelled statistically and described by a standard deviation σ_α. Additionally, free-flying telescopes may experience strong environmental influences. As can be seen from Fig. 5, the input polarizers main axes have to be co-aligned to within $2mrad$ if a rejection ratio of some $60dB$ should be achieved. Requirements on the polarizers themselves are not critical, as elements with a polarization extinction ratio (PXR) of some $60dB$ are commercially available. Depending on the extinction ratio of the input polarizer, a significant wavelength dependence of the rejection ratio occurs if the differences between the desired and the undesired polarization axes differ significantly between the individual arms. Figure 8 shows the results for $\triangle l_p = 20\mu m$. If polarizers with high extinction ratio are used, any rotation of the input polarizers (angle α) has low influence on the rejection ratio if the amplitude control works well. If multiple imperfections are present, the rejection ratio is expected to be smaller than the smallest one caused by each imperfection separately. Figure 9 gives an example, showing the rejection ratio R due to each individual imperfection alone, and due to the combination of all imperfections for the parameters: $\sigma_p = 1nm$, $\sigma_A = 10^{-4}$, $\sigma_\alpha = 10^{-3}rad$, $PXR = 10^3$, and $\triangle l_p = 20\mu m$.

5 Conclusion

The high star light suppression capability of the Robin Laurance interferometer, determined by a broad and deep null of the receive characteristic, requires uniformity of the interferometer arms to a very high degree. To obtain a rejection ratio of $R = 60dB$, as it is required for Sun/Earth-like constellations at an interstellar distance of about 50 light years, maximum standard deviations of only $\sigma_p = 2nm$ and $\sigma_A = 5 \cdot 10^{-4}$ for the differences in optical path length and amplitude transmission can be allowed. Therefore, a successful launch of the DARWIN interferometer, planned by ESA after 2010, requires a large effort in developing new technologies to cope with such instrumental demands.

Acknowledgement

The authors are grateful to Peter J. Winzer for many fruitful discussions and essential contributions to this work.

References

[1] A. Leger et.al., "Could We Search for Primitive Life on Extrasolar Planets in the Near Future? The DARWIN Project", ICARUS **123**, 249–255 (1996)

[2] R.N. Bracewell, R.H. McPhie, "Searching for Nonsolar Planets", ICARUS **38**, 136–147 (1979)

[3] B. Mennesson. J.M. Mariotti, "Array Configurations for a Space Infrared Nulling Interferometer Dedicated to the Search for Earthlike Extrasolar Planets", ICARUS **128**, 202–212 (1997)

[4] O. Wallner, K. Kudielka, W.R. Leeb, "Nulling interferometry for spectroscopic investigation of exoplanets – a statistical analysis of imperfections", The Search for Extraterrestrial Intelligence (SETI) in the Optical Spectrum III (Photonics West), San José (CA/USA), Proc. SPIE **4273**, 47-55 (2001)

[5] A. Karlson, B. Mennesson, "The Robin Laurance nulling interferometers", Proc. SPIE **4006**, 871–880 (2000)

[6] European Space Agency (2001, Sept.), DARWIN project [Online], Available: sci.esa.int/home/darwin

[7] M. Born, E. Wolf, *Principles of Optics*, 7th ed., Cambridge University Press, Cambridge, 1999

Figure 1: Principle of a nulling interferometer (e_1 and e_2 denote the optical field strengths in the interferometer arms).

Figure 2: An artist's conception of the Robin Laurance nulling interferometer for DARWIN.

Figure 3: Geometries and transmission maps of the three sub-interferometers of the Robin Laurance configuration. The different telescope sizes indicate different amplitude transmission factors in the individual interferometer arms. Bright areas in the transmission maps indicate good transmission, while dark areas stand for poor transmission (i.e. suppression). The coordinates are normalized to the planet's position.

Figure 4: General structure of a nulling interferometer with high demands on arm uniformity.

Figure 5: Rejection ratio R in the case of stochastic variations of the optical path lengths (standard deviation σ_p), the amplitude transmissions (standard deviation σ_A), and the input polarizer angle (standard deviation σ_α), and in the case of a finite input polarizer extinction ratio PXR.

Figure 6: Wavelength dependence of the rejection ratio R for different standard deviations σ_p of the stochastically varying optical path lengths.

Figure 7: Wavelength dependence of the rejection ratio R for different standard deviations σ_A of the stochastically varying amplitude transmissions.

Figure 8: Wavelength dependence of the rejection ratio R for different standard deviations σ_α of the stochastically varying input polarizer angles and for different finite extinction ratios. The optical path length differences between the desired and the undesired polarization axes were assumed to differ by $\triangle l_p = 20\mu m$.

Figure 9: Rejection ratio R as a function of the wavelength λ for the combined effect of optical path length and amplitude transmission errors as well as polarization crosstalk. The individual effects are included as reference. The parameters are $\sigma_p = 1nm$, $\sigma_A = 10^{-4}$, $\sigma_\alpha = 1mrad$, $PXR = 10^3$, and $\triangle l_p = 20\mu m$.

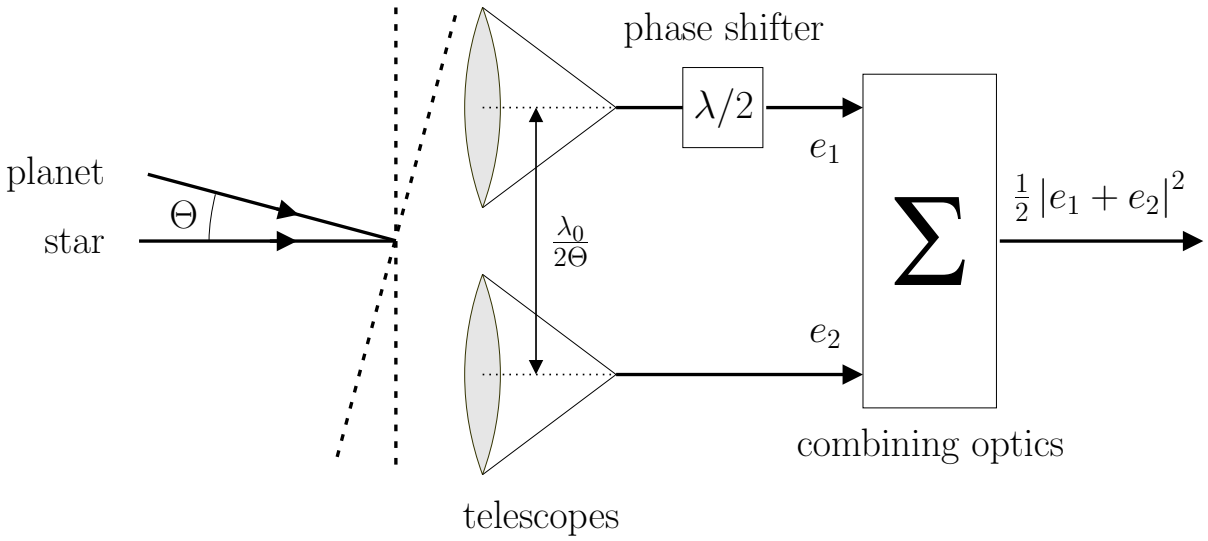
phase shifter
$\lambda/2$
planet
star
Θ
$\frac{\lambda_0}{2\Theta}$
e_1
e_2
$\sum$
$\frac{1}{2}\,|e_1 + e_2|^2$
combining optics
telescopes

Figure 1

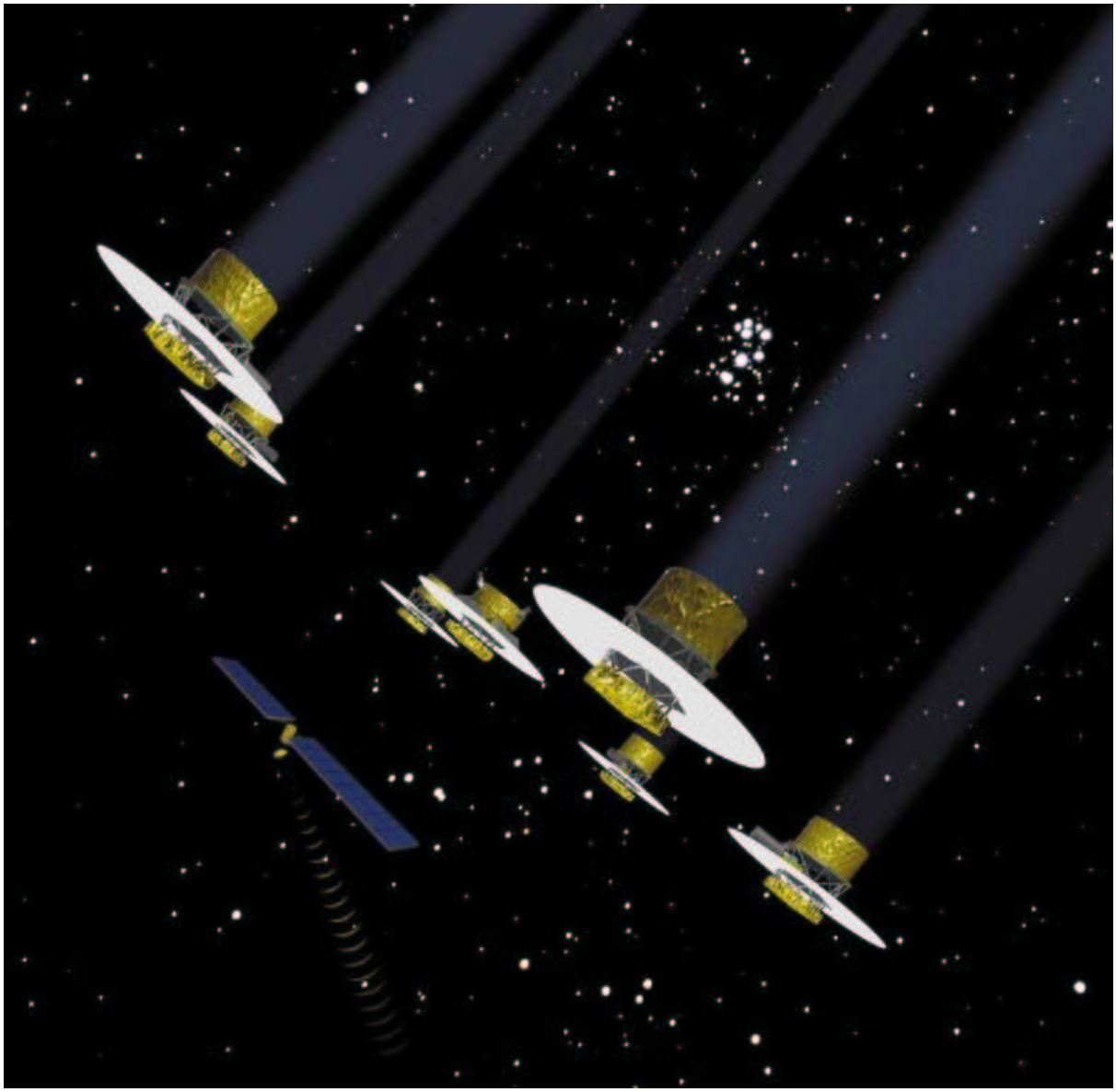

Figure 2

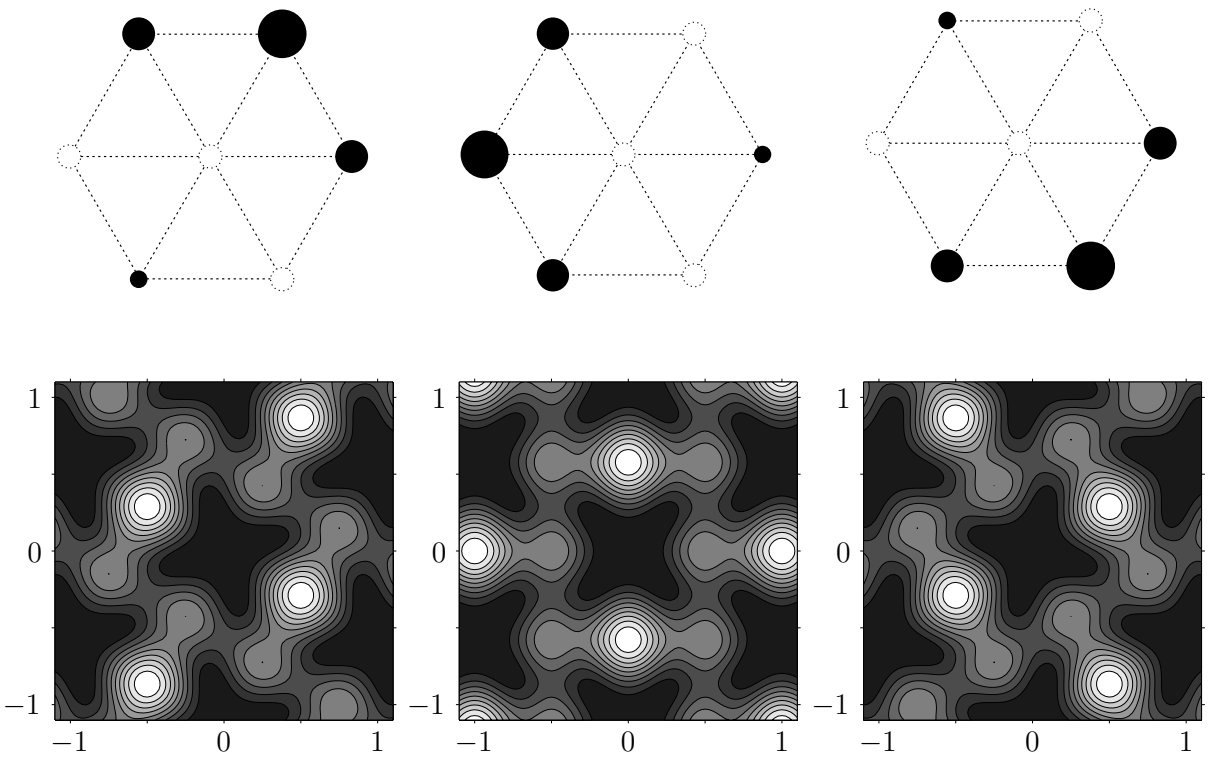

Figure 3

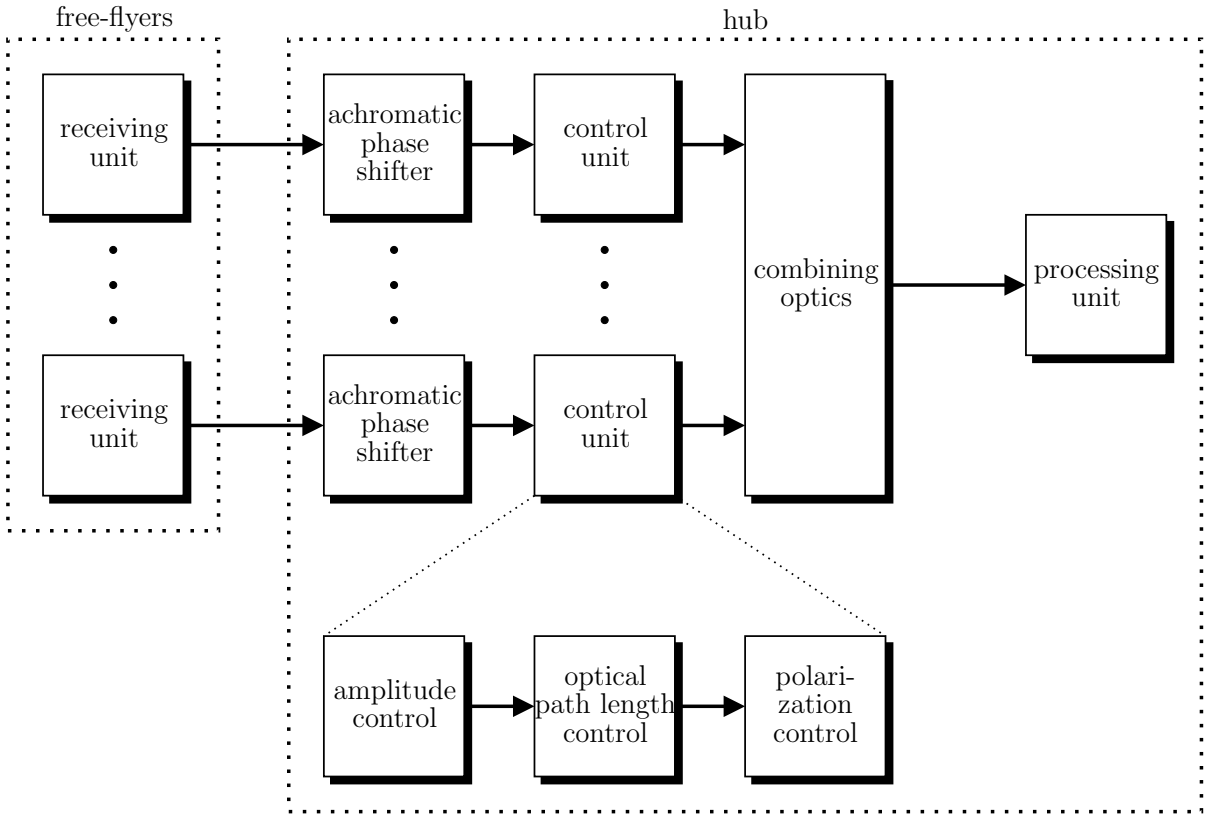
free-flyers
hub
receiving unit
receiving unit
achromatic phase shifter
achromatic phase shifter
control unit
control unit
combining optics
processing unit
amplitude control
optical path length control
polari-zation control

Figure 4

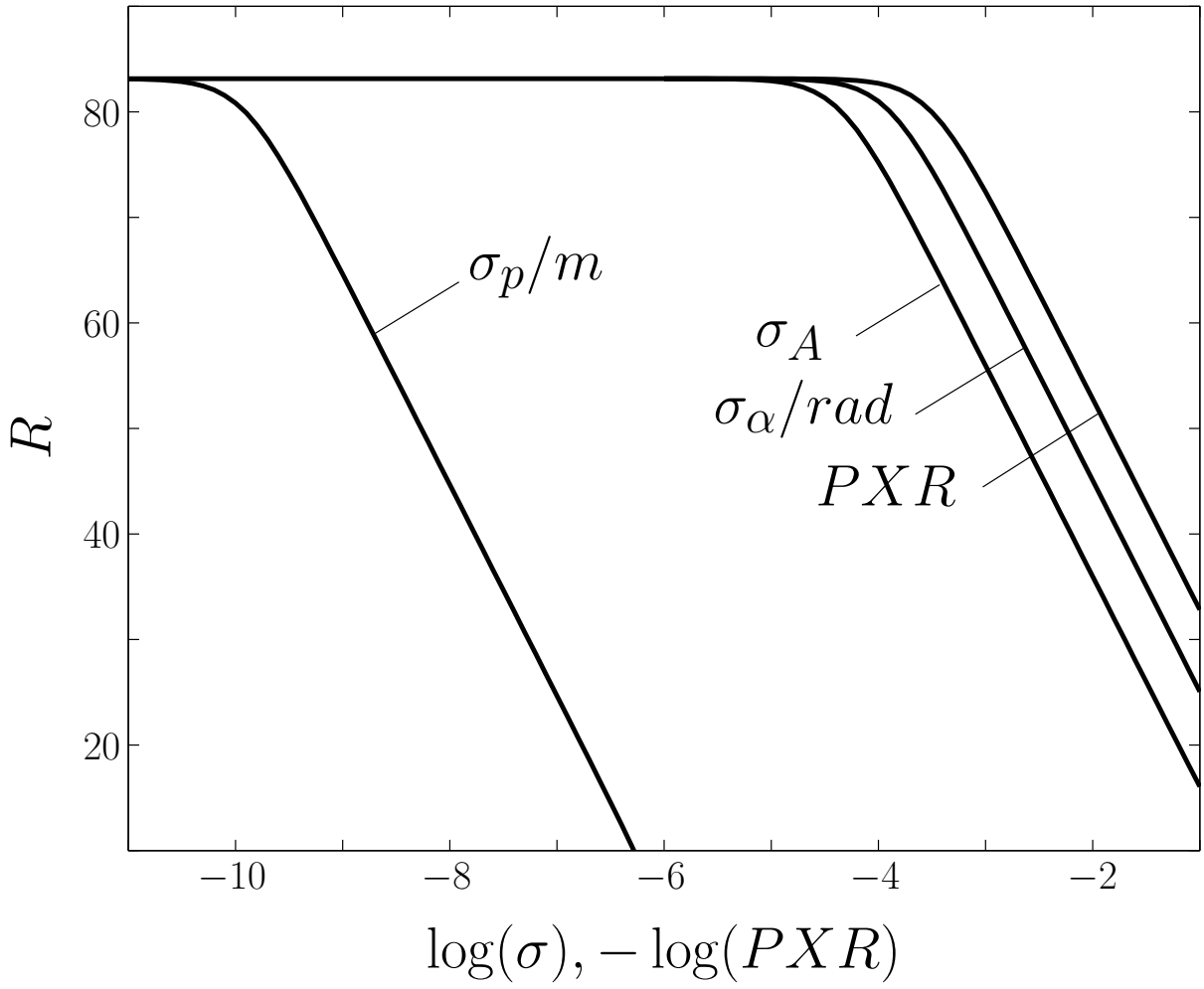

Figure 5

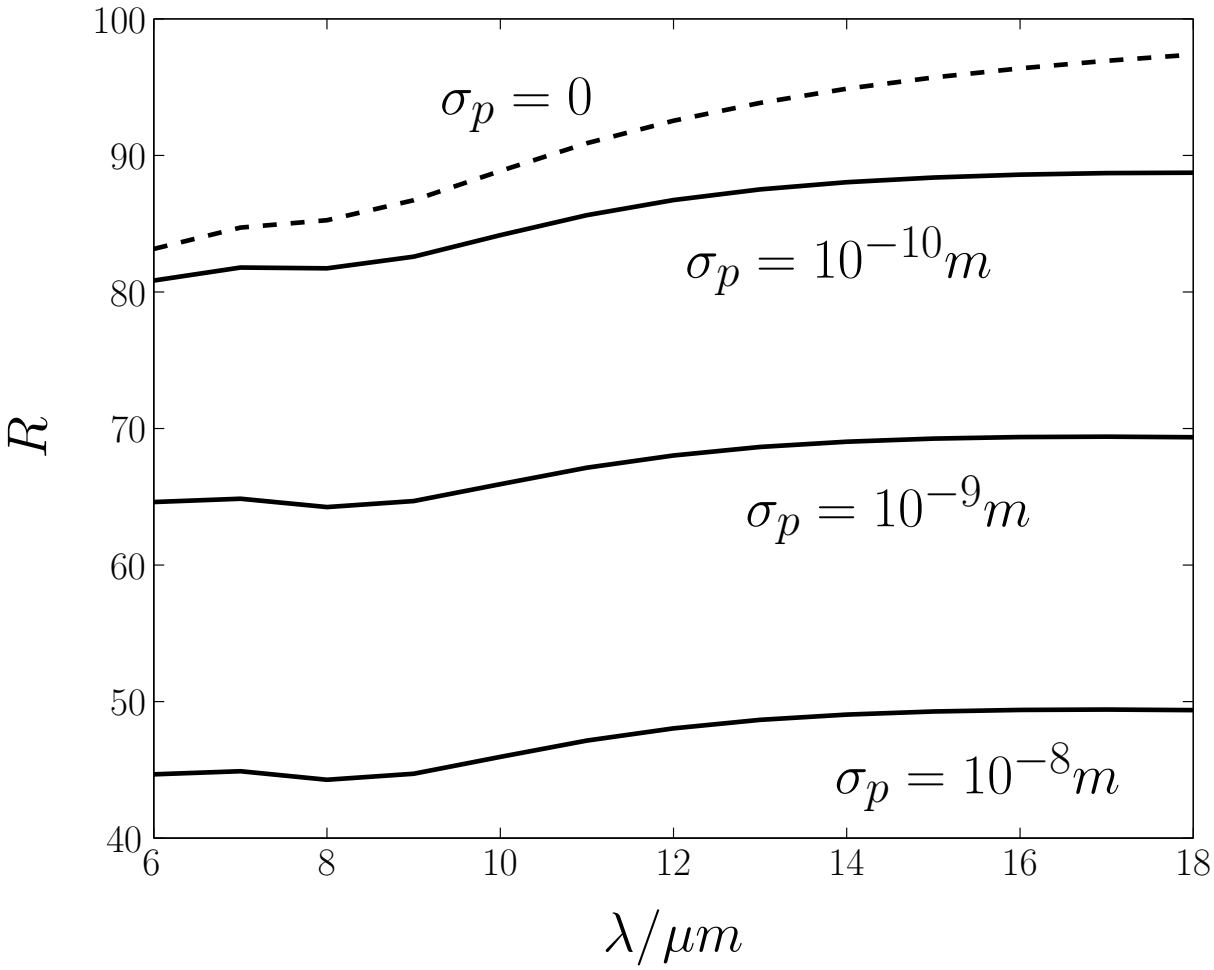
100
90
80
70
60
50
40
6
8
10
12
14
16
18
R
λ/μm
σp = 0
σp = 10−10m
σp = 10−9m
σp = 10−8m

Figure 6

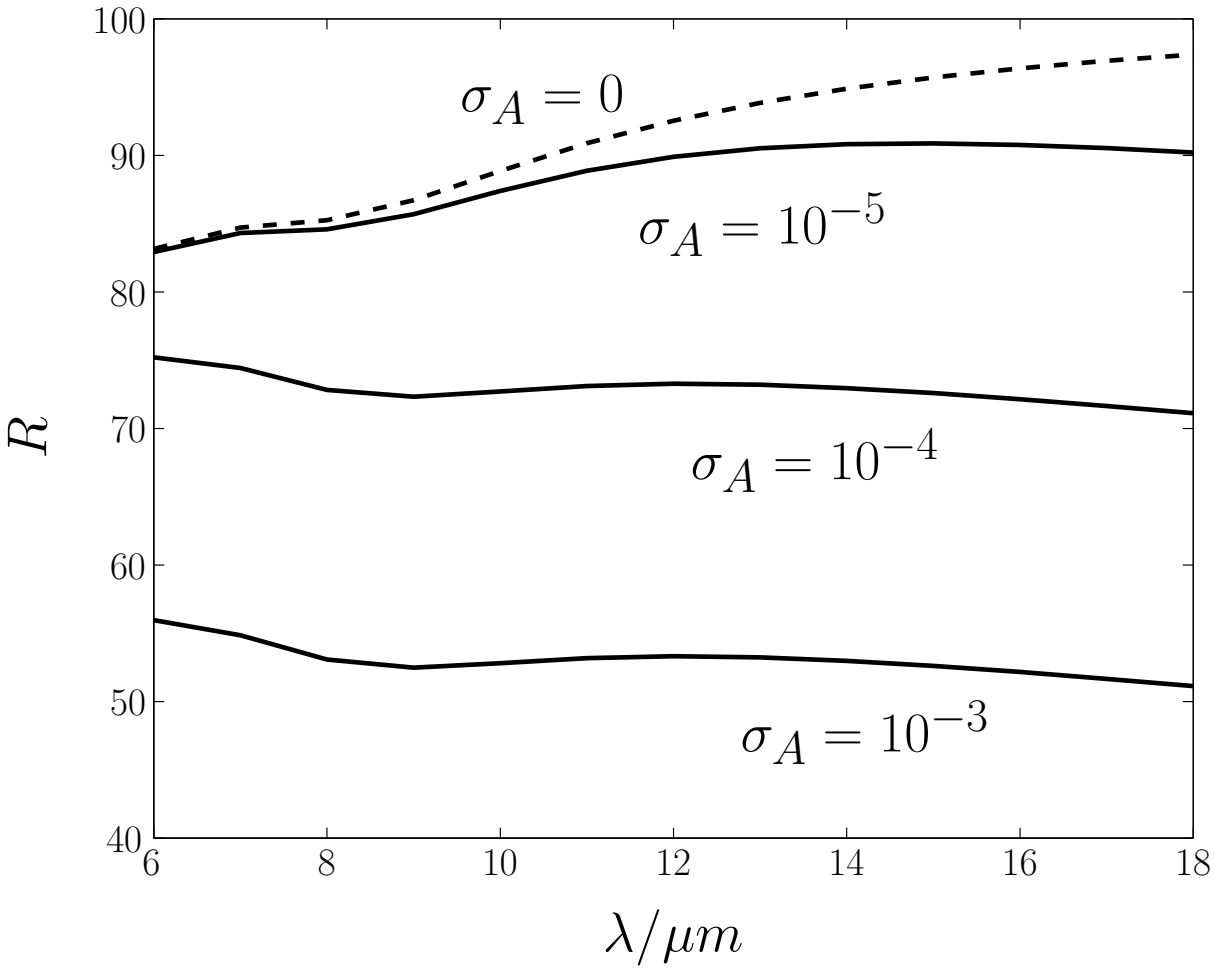

Figure 7

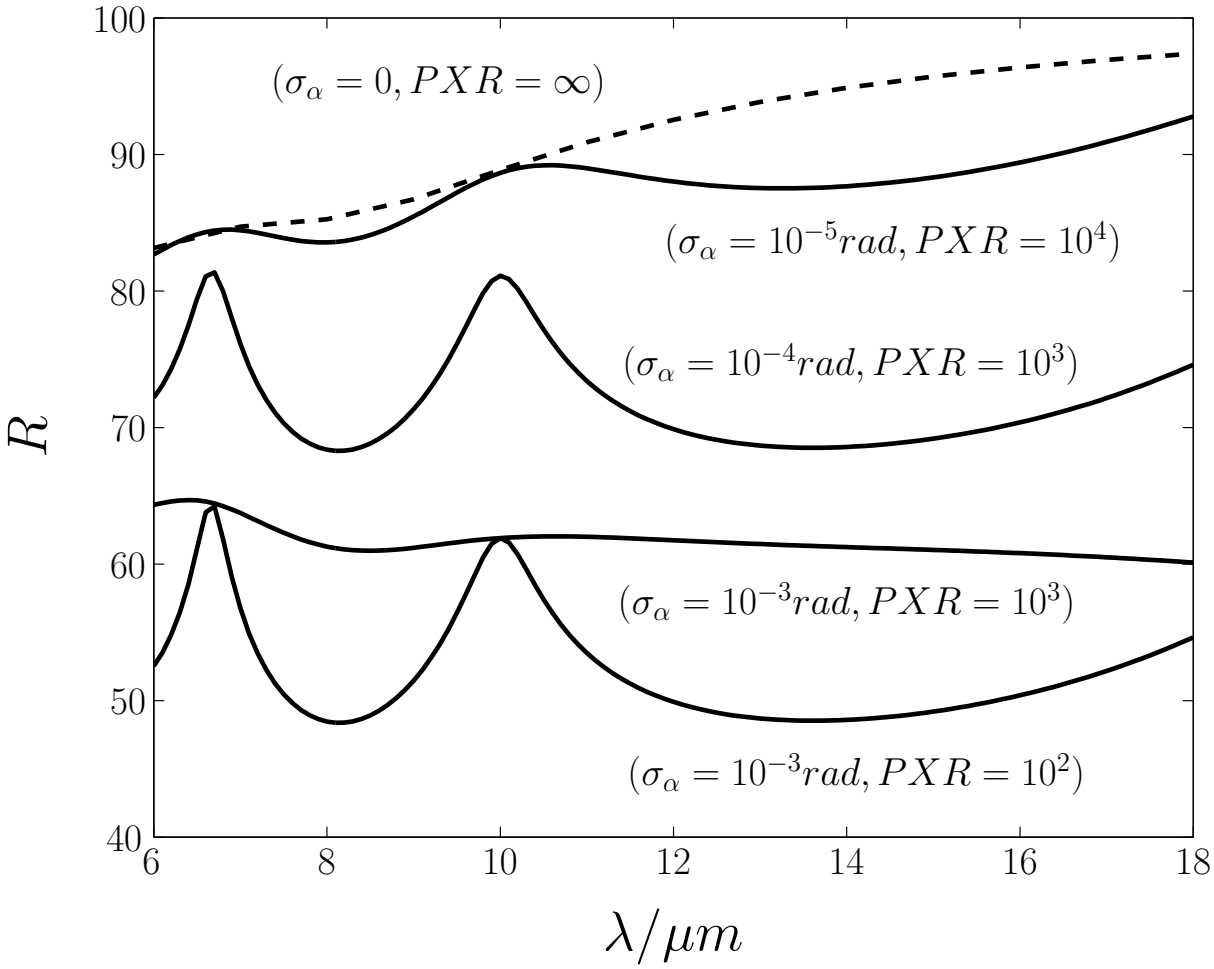
100
90
80
70
60
50
40
6
8
10
12
14
16
18
R
λ/μm
(σα = 0, PXR = ∞)
(σα = 10−5rad, PXR = 10^4)
(σα = 10−4rad, PXR = 10^3)
(σα = 10−3rad, PXR = 10^3)
(σα = 10−3rad, PXR = 10^2)

Figure 8

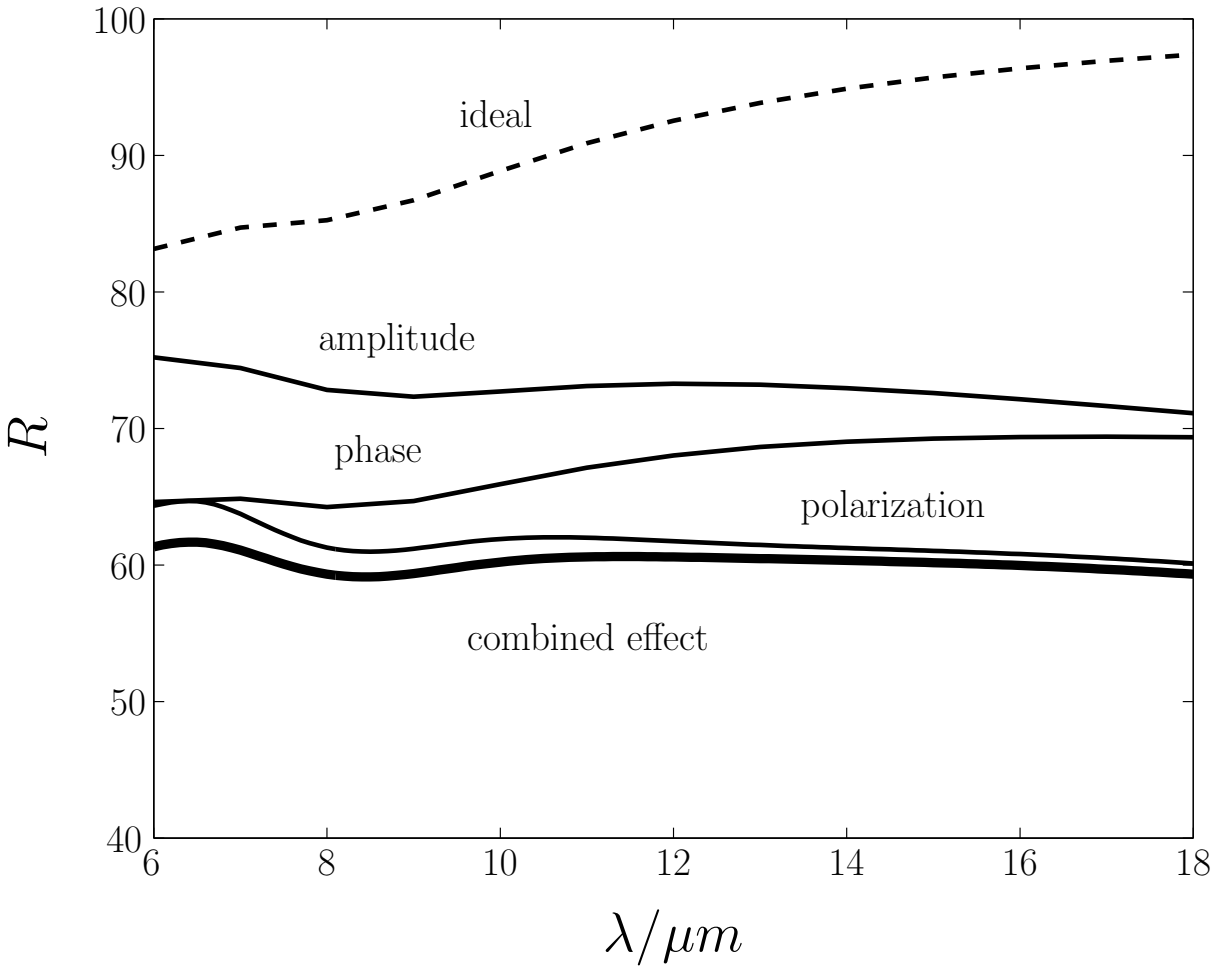
100
90
80
70
60
50
40
R
ideal
amplitude
phase
polarization
combined effect
6
8
10
12
14
16
18
λ/μm

Figure 9